UDC 539.4

# The Effect of Notch Tip Position on the Charpy Impact Energy for Bainitic and Martensitic Functionally Graded Steels

**J. Eskandari Jam,[a] M. Abolghasemzadeh,[b] H. Salavati,[b] and Y. Alizadeh[b,1]**

[a] Composite Center, Malek Ashtar University of Technology, Tehran, Iran

[b] Department of Mechanical Engineering, Amirkabir University of Technology, Tehran, Iran

[1] alizadeh@aut.ac.ir

УДК 539.4

# Влияние положения вершины надреза в образце Шарпи на ударную энергию в функционально-градиентных бейнитно-мартенситных сталях

**Дж. Эскандари Джам[а], М. Аболгасемзаде[б], Х. Салавати[б], И. Ализаде[б,1]**

[а] Центр композитных материалов, Технологический университет им. Малик аль-Аштара, Тегеран, Иран

[б] Механико-машиностроительный факультет, Технологический университет им. Амира Кабира, Тегеран, Иран

*Функционально-градиентные стали, которые относятся к группе функционально-градиентных материалов, обладающих упругопластическими свойствами, получают из аустенитной нержавеющей и малоуглеродистой ферритной сталей путем электрошлаковой переплавки. При использовании функционально-градиентных сталей можно улучшить механические свойства композитов, содержащих мартенситные и бейнитные хрупкие фазы. Представленная аналитическая модель позволяет оценить ударную энергию разрушения образцов Шарпи из бейнитно-мартенситных сталей с учетом зависимости между ударной энергией и размером пластической зоны в вершине надреза. Сравниваются величины ударной энергии для образцов Шарпи из функционально-градиентных сталей и однородного материала, соответствующего слою материала вблизи вершины надреза. С использованием программного комплекса ABAQUS выполнено трехмерное конечноэлементное моделирование данного процесса. Согласно закону Холломана для пластической зоны получены характеристики материала в различных его слоях. Рассматривалось экспоненциальное изменение характеристик материала по ширине образца. Предложенная модель позволяет получить результаты, хорошо согласующиеся с имеющимися экспериментальными данными и результатами конечноэлементных расчетов.*

***Ключевые слова***: функционально-градиентная сталь, энергия разрушения образцов Шарпи, положение вершины надреза, размер пластической зоны, метод конечных элементов.

**Introduction**. Failure phenomena in continuum media, either solids or liquids, can be regarded as a single physical phenomenon, which mathematically can be identified by the fulfilment of a limit condition usually involving the stressed state of the material [1]. Functionally graded (FG) materials are the advanced materials in the family of engineering composites made of two or more constituent phases in which the composition, structure and/or specific properties vary continuously and smoothly in the preferred direction to produce combinations of properties that could not be achieved through monolithic materials composed of similar constituents. In this regard, well-known metal-ceramic FG materials are mostly used to enhance the properties of thermal-barrier systems, because cracking or

delamination, which are often observed in conventional multi-layer systems, are avoided due to the smooth transition between the properties of the components [2].

Compositionally graded steels are an interesting development and a new area of interest among steel researchers. These new materials allow for superior combinations of strength and ductility when compared to traditional high-strength steels. Chehab et al. [3] show the potential for developing architectured structures in steels using decarburization method. They also show a potential for the control of instabilities such as necking or damage and fracture events.

In addition, a special class of multiphase materials with graded microstructure can be obtained at cryogenic temperatures as a result of smooth transition from the parent phase to the secondary phase. The required continuously graded material features are obtained at low temperatures via the mechanism of controlled strain-induced phase transformation from the purely austenitic phase with face cubic centred (fcc) lattice to the martensitic phase with body cubic centred (bcc) lattice by imposing kinematically controlled torsion on a stainless steel bar until the material starts transforming itself close to the outside radius of the bar [4].

More recently, other types of functionally graded steels (FGS) have been produced from austenitic stainless steel and plain carbon steel by controlling the chemical distribution of chromium, nickel and carbon atoms at the remelting stage through electroslag remelting (ESR) process [5]. Studies on transformation characteristics of FGSs produced via ESR have shown that by selecting appropriate arrangement and thickness of original electrodes made of ferritic and austenitic steels, composites with graded ferritic and austenitic regions together with emerged bainitic and/or martensitic layers can be obtained:

$$(\alpha_0\gamma_0) \xrightarrow{ESR} (\alpha\beta\gamma),$$
$$(\gamma_0\alpha_0\gamma_0) \xrightarrow{ESR} (\gamma M\gamma),$$
$$(\alpha_0\gamma_0\alpha_0\gamma_0) \xrightarrow{ESR} (\alpha\beta\gamma M\gamma),$$
$$(\alpha_0\gamma_0\gamma_0\alpha_0) \xrightarrow{ESR} (\alpha\beta\gamma\beta\alpha),$$

where $\alpha_0$ and $\gamma_0$ are original ferritic and austenitic stainless steels in the primary electrode, respectively, $\alpha$ and $\gamma$ are ferritic and austenitic graded regions in the final composite, respectively, and $\beta$ and $M$ are emerged bainitic and martensitic layers in the final composite, respectively.

In some previous studies, the tensile behavior of FGSs with different configurations was experimentally investigated and modeled by modified rule of mixture [6]. In that work, variation of yield strength in the graded region has been estimated by means of a linear expression between the yield strength gradient and the Vickers microhardness profile of the composite. In particular, Vickers microhardness profile of austenitic graded region of the $\alpha\beta\gamma$ FGSs has been modeled utilizing the mechanism-based strain gradient plasticity (MSG) theory [7]. Afterwards, the MSG theory was used to model the tensile strength of FGSs [8]. The main advantage of this modified model with respect to the previous one [6] is that the microhardness of each layer (i.e., Vickers microhardness profile) is not required for determining the mechanical properties of the FGSs.

Other important aspects are related to the characterization of FGSs under hot-working conditions. In [9], the flow stress of FGSs under hot compression loading was assessed by applying constitutive equations in combination with the rule of mixture. In this paper, a theoretical model has been proposed to assess the flow stress of bainitic $\alpha\beta\gamma$ and martensitic $\gamma M\gamma$ graded steels under hot compression conditions based on the Reuss model for the overall strains.

The brittle or quasi-brittle static failure of U-notched plates made of $\gamma M\gamma$ FGS, in which the properties gradient is parallel to the notch depth, was studied by Barati et al. [10]. As remarked in that work, when the notch tip is placed in the transition region between austenite and martensite layers, the fracture load in FGS is higher than that of the homogeneous steel. On the other hand, when the notch is placed in the transition region between martensite and austenite layers, the fracture load of the homogeneous steel is greater than that of FGS. In that study, the Young modulus and Poisson's ratio have been assumed to be constant, while the ultimate tensile strength and the fracture toughness $K_{\mathrm{I}c}$ vary exponentially through the specimen width. The effect of the notch depth on the critical fracture load has also been also investigated therein.

In [11–13], the Charpy impact energy of crack divider specimens was measured experimentally and modelled by two methods. The obtained results showed that the Charpy impact energy of the specimens depended on the type and the volume fraction of the present phases. In both theoretical methods, Charpy impact energy of the FGS was considered to be the sum of the Charpy impact energy of constituent layers by means of the rule of mixtures. One mehod correlates the Charpy impact energy of FGSs to the Charpy impact energy of the individual layers through Vickers microhardness of the layers [11]. In the other work, the Charpy impact energy for all layers was related to the area under the stress–strain curve measured in plain tensile test [12, 13].

In addition, the Charpy impact energy [14–16] of both ferritic and austenitic graded regions of $\alpha\beta\gamma$ FGS in the form of crack divider configuration has been assessed by a same methodology proposed in previous works [11–13] and using the MSG theory. In these works, the flow stress (yield strength and/or ultimate tensile strength) of each layer has been related to the density of the dislocations of that layer and by assuming the Holloman relation for the corresponding stress–strain curve, the whole stress–strain curve of that layer were determined.

Following parallel tracks, the Charpy impact energy of FGSs produced by ESR process in the form of crack arrester configuration has also been investigated in [17]. The results obtained in that study for $\alpha\beta\gamma$ and $\gamma M\gamma$ composites indicate that the notch tip position with respect to the bainite or martensite layer significantly affects the Charpy impact energy of FGSs. The closer the notch tip to the tougher layer (median bainitic or martensitic layers), the higher is the Charpy impact energy of the composite due to increment of energy absorbed by the plastic deformed zone ahead of the notch and vice versa [17].

As stated in [17] for arrester configuration, no precise mathematical modelling was presented to correlate the Charpy impact energy of FGSs to the morphology of each layer. This is an actual gap in the literature. The main aim of the present work is to fill this gap and provide a new analytical model for the assessment of the Charpy impact energy of FGSs in the form of crack arrester configuration. Moreover, three-dimensional finite element (FE) analysis by ABAQUS software was performed to simulate the Chapry impact energy process of FGS specimens in the form of crack arrester configuration. Since the most plastic deformation has been concentrated on the notch tip zone, the notch tip area has been partitioned with a fine mesh. The stress–strain curve of layers in functionally graded composite corresponding to partitions in FE model, was obtained from MSG theory and was fed into the model as constitutive behavior. The outputs of the proposed model for different notch tip positions of $\alpha\beta\gamma$ and $\gamma M\gamma$ FGS are compared with the experimental results taken from the recent literature and those obtained from the simulation.

1. **Analytical Model**. In investigation of Charpy impact response of FGS, there are two common configurations consisting of crack divider and crack arrester forms as illustrated in Fig. 1a and 1b, respectively. Crack divider configuration is the case where the plane which contains the notch tip is perpendicular to the layers, and crack arrester configuration is the case where the plane which contains the notch tip is parallel to the layers.

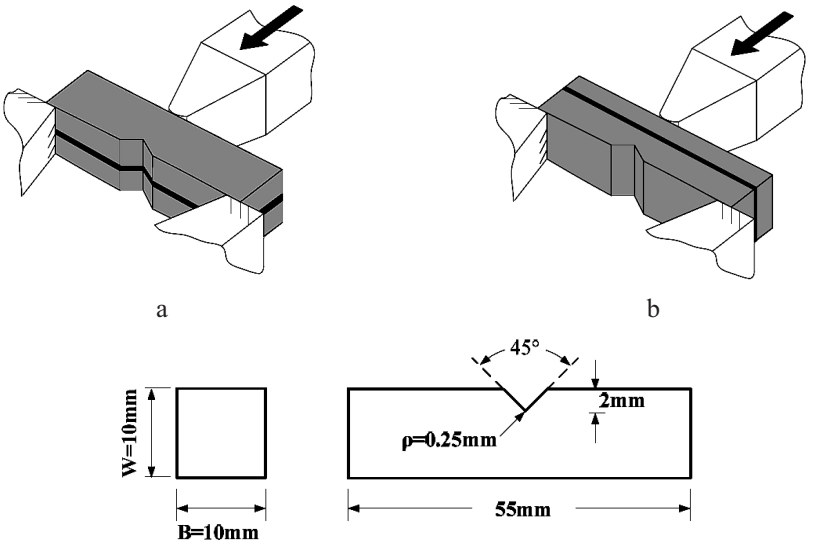


Fig. 1. The schematic representation of configuration of composite Charpy test specimens in the form of crack divider (a) and crack arrester (b); the geometry of Charpy specimens (c).

In [17], the effect of the distance between the notch tip and the position of the median phase on the Charpy impact energy is investigated. The results show that in the transition region between original ferrite and bainite layer of $\alpha\beta\gamma$ composite, when the notch apex is close to the median layer, the impact energy reaches its maximum value due to the increment of the absorbed energy by plastic deformation ahead of the notch tip (i.e., positive toughness slope; see Fig. 2a). On the other hand, when the notch apex is far from the median layer, the impact energy strongly decreases. While, in the transition region between original austenite and bainite layer of $\alpha\beta\gamma$ composite as well as in the transition region between original austenite to martensite layer of $\gamma M\gamma$ composite, when the notch apex is close to the median layer, the impact energy reaches its minimum value due to decrease of the absorbed energy by plastic deformation ahead of the notch tip (i.e., negative toughness slope; see Fig. 2b).

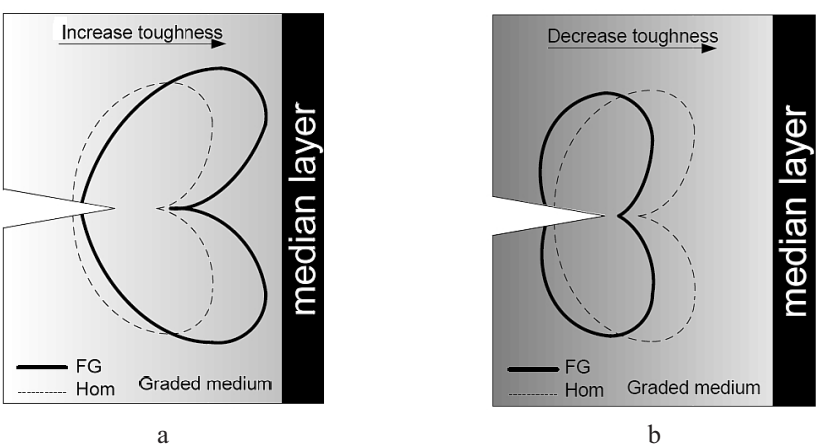


Fig. 2. Comparision between notch tip plastic zone of homogeneous medium and graded one positive (a) and negative (b) toughness slope.

Due to the lack of explicit equations to determine absorbed energy in the Charpy impact test, we attempt to propose a model regarding empirical relationships that have been determined to correlate the Charpy impact energy of monotonic materials to the other characteristic properties. To this end, the relationships between Vickers microhardness and the Charpy impact energy, as well as expression between the fracture toughness, yield strength and Charpy impact energy are considered as follows [18–20]:

$$CV = C_1 \frac{CV}{VH} + C_2, \tag{1}$$

$$C_3 \frac{CV}{\sigma_Y} + C_4 = \beta'(K_{\mathrm{I}c}/\sigma_Y)^2, \tag{2}$$

where $CV$ denotes Charpy impact energy and $VH$ stands for Vickers microhardness, $K_{\mathrm{I}c}$ and $\sigma_Y$ are the fracture toughness and yield strength, respectively, and $\beta'$, $C_1$, $C_2$, $C_3$, and $C_4$ are material constants.

By attention to the linear relationship between the Vickers hardness and the yield strength [6, 21], it can be seen that the right-hand side of Eq. (1) can be explicitly expressed as a function of the term $(K_{\mathrm{I}c}/\sigma_Y)^2$ according to Eq. (2). Now, the combination of Eqs. (1) and (2) allow us to suppose that the Charpy impact energy is proportional to $(K_{\mathrm{I}c}/\sigma_Y)^2$ term. On the other hand, the radius of plastic region in the vicinity of crack tip [see Eq. (3)], $r_y$, is proportional to $(K_{\mathrm{I}c}/\sigma_Y)^2$ (see [20])

$$r_y = \alpha' \left(\frac{K_{\mathrm{I}c}}{\sigma_Y}\right)^2 \cos^2\left(\frac{\theta}{2}\right)\left[(1-2\nu)^2 + 3\sin^2\left(\frac{\theta}{2}\right)\right], \tag{3}$$

where $\nu$ is Poisson's ratio and $\alpha'$ is a constant. Note that Eq. (3) is valid for the plastic radius of a homogeneous material under plane strain conditions and mode I loading considering the von Mises yield criterion.

Consequently, the simple relationship between the Charpy impact energy and the size of the plastic region can be written in the following form:

$$CV = N_1 r_y + N_2, \tag{4}$$

where $N_1$ and $N_2$ are constants, which depend only on the material. Equation (4) is the basis of the proposed model because it shows the proportionality between the Charpy impact energy and the size of the plastic region in the vicinity of crack tip.

For the purpose of modeling the Charpy impact of a functionally graded composite, the graded layers has been divided into thin elements with the homogeneous properties. As explained earlier, the Charpy impact energy of a homognous material is related to the radius of the plastic zone with Eq. (4). This relation could be developed for graded materials. Therefore, we suppose that the Eq. (4) is acceptable for a graded region as follows:

$$CV(x) = N_1^{FGS} r_y(x) + N_2^{FGS}. \tag{5}$$

The constants $N_1^{FGS}$ and $N_2^{FGS}$ will be determined according to the boundary condition:

$$\begin{aligned} x = x_1 &\Rightarrow CV = CV_{(1)}, \quad r_y = r_{y(1)}, \\ x = x_2 &\Rightarrow CV = CV_{(2)}, \quad r_y = r_{y(2)}. \end{aligned} \tag{6}$$

Equation (3) shows that the plastic region size varies as a function of the angle $\theta$. In order to eliminate the effect of the angle on the size of the plastic region, the following equation is proposed here to assess the Charpy impact energy of the graded region:

$$CV_{FG} = N_2^{FGS} + \sqrt{\left(\frac{\Omega_{FG}}{\Omega_H}\right)}(CV_H - N_2^{FGS}). \tag{7}$$

According to Eq. (7), the Charpy impact energy of a FGS, $CV_{FG}$, depends on the distance of the notch tip from the middle phase, $d$, and on the type of the considered composite. The term $CV_H$ is the Charpy impact energy of the element containing the notch tip, $\Omega_H$ is the area of the plastic region for a homogeneous specimen composed exclusively of the material forming the element containing the notch tip, $\Omega_{FG}$ is the area of the plastic region for a FGS specimen, in which the mechanical properties vary along the direction of the notch bisector line, and $N_2^{FGS}$ is a constant that was determined by imposing the appropriate boundary conditions.

In order to determine the profile of the notch tip plastic region, a specimen shown in Fig. 3 with the notch depth $a = 2$ mm and the notch opening angle $2\alpha = 45°$ with accordance to the Charpy standard test specimen has been considered.

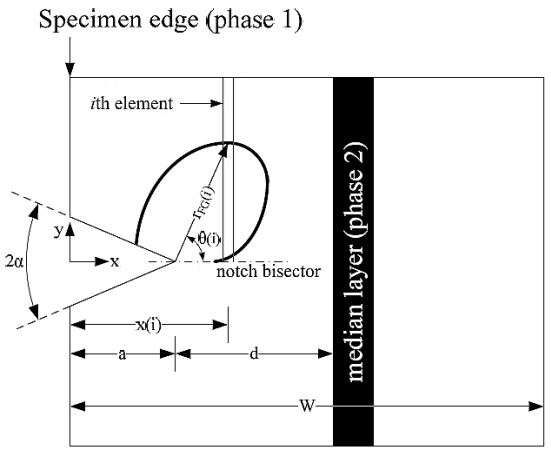


Fig. 3. The schematic representation profile of the notch tip plastic region for the crack arrester configurtaion of FGS.

The yield strength $\sigma_Y$ and fracture toughness $K_{\mathrm{I}c}$ have been supposed to vary exponentialy along the notch bisector line (i.e., $x$-direction in Fig. 3)

$$K_{\mathrm{I}c}(x) = (K_{\mathrm{I}c})_0 \exp\left[\frac{x}{d+a}\ln\left(\frac{K_{\mathrm{I}c(2)}}{K_{\mathrm{I}c(1)}}\right)\right], \tag{8}$$

$$\sigma_Y(x) = (\sigma_Y)_0 \exp\left[\frac{x}{d+a}\ln\left(\frac{\sigma_{Y(2)}}{\sigma_{Y(1)}}\right)\right]. \tag{9}$$

In Eqs. (8) and (9), $x$ is the distance of the element from the specimen edge and indices 1 and 2 are related to the mechanical properties of the specimen edge and the middle bainitic phase, respectively (see Fig. 3). It is clear that yield strength and the

fracture toughness of the elements ahead of the notch tip could be obtained using $a = 2\,\text{mm}$ in the Eqs. (8) and (9). Therefore, considering the Eqs. (3), (8), and (9), the area surrounding the plastic region ahead of the notch tip for the homogeneous material could be obtained as follows:

$$\Omega_H = 2\left[\frac{1}{2}\int_{\theta=0}^{\theta=\pi}(r_H(\theta))^2\,d\theta\right] =$$

$$= \alpha'^2\left(\frac{K_{\text{Ic}}}{\sigma_Y}\right)^4\int_{\theta=0}^{\pi} f(\theta)^2\,d\theta = \alpha'^2\left(\frac{D_1}{D_3}\right)^4 \exp[4a(D_2 - D_4)]I_1, \tag{10}$$

in which

$$D_1 = K_{\text{Ic}(1)}, \qquad D_2 = \frac{1}{d+a}\ln\left(\frac{K_{\text{Ic}(2)}}{K_{\text{Ic}(1)}}\right), \qquad D_3 = \sigma_{Y(1)}, \qquad D_4 = \frac{1}{d+a}\ln\left(\frac{\sigma_{Y(2)}}{\sigma_{Y(1)}}\right),$$

$$I_1 = \int_0^{\pi}\left\{\cos^2\frac{\theta}{2}\left[(1-2\nu)^2 + 3\sin^2\frac{\theta}{2}\right]\right\}^2 d\theta.$$

The value of angular integral $I_1$ is independent of the composite type, as well as the distance $d$, and it is equal to 2.2594 for all cases.

Since $(K_{\text{Ic}}/\sigma_Y)^2$ varies for different elements, the effect of angle and position must be considered to determine the area surrounding the plastic region ahead of the notch for the graded specimen $\Omega_{FG}$. For example, an element with the distance $x_{(i)}$ from the specimen edge called the $i$th element with the radius $r_{FG(i)}$ and the angle of the plastic region boundary $[\theta_{(i)}]$ is shown in Fig. 3. Considering Eq. (3), $r_{FG(i)}$ is calculated as follows:

$$r_{FG(i)} = \alpha' H(x_{(i)}) f(\theta_{(i)}), \tag{11}$$

where

$$H(x_{(i)}) = \left(\frac{K_{\text{Ic}}(x_{(i)})}{\sigma_Y(x_{(i)})}\right)^2 = \left(\frac{D_1}{D_3}\right)^2 \exp[2x_{(i)}(D_2 - D_4)], \tag{12}$$

$$f = \cos^2\left(\frac{\theta_{(i)}}{2}\right)\left[(1-2\nu)^2 + 3\sin^2\left(\frac{\theta_{(i)}}{2}\right)\right], \tag{13}$$

where $K_{\text{Ic}}(x_{(i)})$ and $\sigma_Y(x_{(i)})$ are the fracture toughness and the yield strength of the $i$th element, respectively.

Moreover, with reference to the Fig. 3, Eq. (14) correlates the radius, the angle of the plastic region and the position of the $i$th element as follows:

$$x_{(i)} - a = r_{FG(i)}\cos(\theta_{(i)}). \tag{14}$$

By combination of Eqs. (11) and (14), one obtains

$$\frac{x_{(i)} - a}{H(x_{(i)})} = \alpha' f(\theta_{(i)})\cos(\theta_{(i)}). \tag{15}$$

In order to simplify the calculation, we consider $\exp(x)=1+x+O(x^2)$ for the function $H$ in Eq. (12) utilizing Taylor series and neglecting the higher-order terms. Therefore, $x_{(i)}$ is calculated from Eq. (15) in terms of $\theta_{(i)}$ as follows:

$$x_{(i)}=\frac{a+A}{1-2B}, \tag{16}$$

where

$$A=\alpha'\left(\frac{D_1}{D_3}\right)^2 f(\theta_{(i)})\cos(\theta_{(i)}), \tag{17}$$

$$B=\alpha'\left(\frac{D_1}{D_3}\right)^2 (D_2-D_4)f(\theta_{(i)})\cos(\theta_{(i)}). \tag{18}$$

Now, substituting $x_{(i)}$ from Eq. (16) into Eq. (11), $r_{FG(i)}$ in terms of $\theta_{(i)}$ is obtained as follows:

$$r_{FG}(\theta_{(i)})=\alpha'\left(\frac{D_1}{D_3}\right)^2 f(\theta_{(i)})\left[1+\frac{2(a+A)}{1-2B}(D_2-D_4)\right]. \tag{19}$$

By integration from Eq. (19), $\Omega_{FG}$ is determined as follows:

$$\Omega_{FG}=\int_0^{\pi} r_{FG}^2(\theta)d\theta=\alpha'^2\left(\frac{D_1}{D_3}\right)^4\{I_1+(D_2-D_4)I_2+(D_2-D_4)^2 I_3\}. \tag{20}$$

The angular integrals $I_2$ and $I_3$ in Eq. (20) are as follows:

$$I_2=\int_0^{\pi}\left\{\frac{4(a+A)}{1-2B}\left(\cos^2\frac{\theta}{2}\left[(1-2\nu)^2+3\sin^2\frac{\theta}{2}\right]\right)^2\right\}d\theta, \tag{21}$$

$$I_3=\int_0^{\pi}\left\{\left(\frac{2a+2A}{1-2B}\right)^2\left(\cos^2\frac{\theta}{2}\left[(1-2\nu)^2+3\sin^2\frac{\theta}{2}\right]\right)^2\right\}d\theta. \tag{22}$$

Note that $I_2$ and $I_3$ contain the parameters $A$ and $B$, which are related to the boundary condition of composites [see Eqs. (17) and (18)]. Therefore, the values of $I_2$ and $I_3$ must be calculated for different types of graded regions. Moreover, the values of these integrals are independent of the notch tip position. Meanwhile, the constant $N_2^{FGS}$ is calculated as follows:

$$N_2^{FGS}=\frac{r_{y(1)}CV_{H(2)}-r_{y(2)}CV_{H(1)}}{r_{y(1)}-r_{y(2)}}. \tag{23}$$

Finally, substituting Eqs. (10), (20), and (23) into Eq. (7), the impact energy of FGS is obtained as follows:

$$CV_{FG} = \frac{\left(\frac{K_{Ic(1)}}{\sigma_{Y(1)}}\right)^2 CV_{H(2)} - \left(\frac{K_{Ic(2)}}{\sigma_{Y(2)}}\right)^2 CV_{H(1)}}{\left(\frac{K_{Ic(1)}}{\sigma_{Y(1)}}\right)^2 - \left(\frac{K_{Ic(2)}}{\sigma_{Y(2)}}\right)^2} +$$

$$+ \left( \frac{I_1 + \frac{I_2}{d+a} \ln\left(\left[\frac{K_{Ic(2)}}{K_{Ic(1)}}\right] \Big/ \left[\frac{\sigma_{Y(2)}}{\sigma_{Y(1)}}\right]\right) + \frac{I_3}{(d+a)^2} \ln^2\left(\left[\frac{K_{Ic(2)}}{K_{Ic(1)}}\right] \Big/ \left[\frac{\sigma_{Y(2)}}{\sigma_{Y(1)}}\right]\right)}{I_1 \left(\left[\frac{K_{Ic(2)}}{K_{Ic(1)}}\right] \Big/ \left[\frac{\sigma_{Y(2)}}{\sigma_{Y(1)}}\right]\right)^{4a/(d+a)}} \right)^{1/2} \times$$

$$\times \left( CV_H - \frac{\left(\frac{K_{Ic(1)}}{\sigma_{Y(1)}}\right)^2 CV_{H(2)} - \left(\frac{K_{Ic(2)}}{\sigma_{Y(2)}}\right)^2 CV_{H(1)}}{\left(\frac{K_{Ic(1)}}{\sigma_{Y(1)}}\right)^2 - \left(\frac{K_{Ic(2)}}{\sigma_{Y(2)}}\right)^2} \right). \quad (24)$$

According to Eq. (24), the Charpy impact energy of FGS is obtained as a function of the notch depth, the notch tip position and the boundary condition of the region that conclude the notch tip. In this paper, Eq. (24) has been used to determine the Charpy impact energy of two kinds of FGS with different notch tip positions, while the notch depth is kept constant.

2. **Finite Element Analysis**. The commercial finite element analysis software ABAQUS 6.11 is employed to simulate the Charpy impact process. The geometry and dimension of the studied notched specimen is in accordance with the Charpy standard impact test as illustrated in Fig. 1c.

In the studied FGS, the elastic properties, as well as mass density, are considered to be constant in the whole composie, while the gradient will appear in the plastic part of the stress–strain curve. Therefore, the whole specimen except the notch tip zone in which considerable plastic deformation occurs, has been considered to be homogeneous with elastic properties. The notch tip region, which contains the most plastic deformation, has been partitioned in the properties' gradient direction (Fig. 4a). The stress–strain curve of each layer in the partition has been obtained by the procedure explained in [16]. In this method, Hooke's law and the Holloman model are used to describe the elastic and plastic parts of stress–strain curve, respectively. Moreover, the yield strength, the ultimate strength and the strain hardening exponent were considred to vary exponentially in the graded region.

The values of the Young modulus, Poisson's ratio, and mass density were considered to be constant for all partitions as 207 GPa, 0.33, and 7800 kg/m$^3$, respectively. The C3D8R cubic elements were joined together to build the standard Charpy impact specimen, and a tiny mesh in the notch tip region was considered to have the maximum accuracy (Fig. 4b).

The distance between the supports were considered to be 40 mm in accordance with Charpy standard test. Also, a hammer was modeld with a rigid body of 20 kg weight. Figure 5 shows the simulated model of the process. Moreover, the dynamical loading was selected with the 5.42 m/s velocity of the hammer such that the initial energy of the hammer was 300 J in accordance with the Charpy standard test.

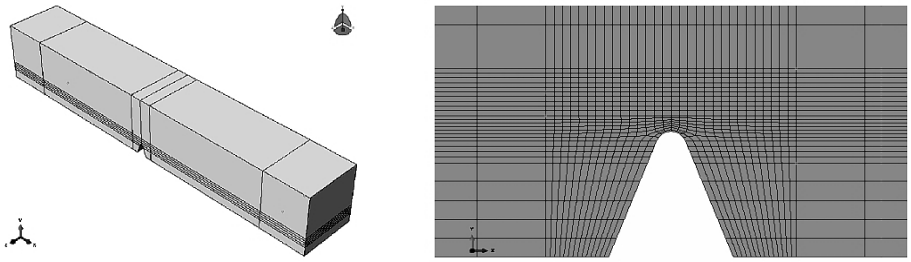

a b

Fig. 4. The simulated model in the ABAQUS software: (a) the partition around the notch; (b) mesh around the notch.

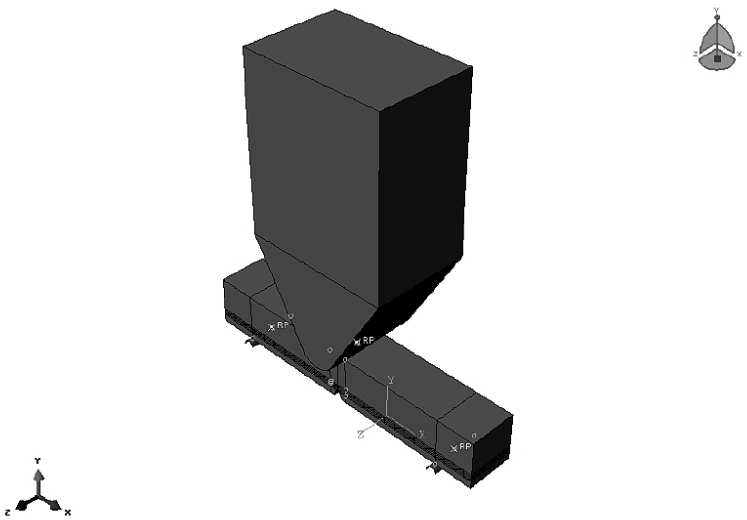

Fig. 5. Three dimentional FE model of the Charpy impact process.

The energy transferred to the Charpy specimen during impact is dissipated and stored in different forms. In general, the total absorbed energy in the Charpy test can be considered as summation of the dissipated energy due to the plastic deformation and the necessary enegy to propagate the crack until fracture. This condition could be observed in the tests performed on the notched and cracked specimens (like the Charpy standard test). In the Chapry impact test, the main part of the plastic deformation is supposed to occur around the notch tip before the crack initiation, while with the crack propagation until fracture may be considered to be elastic. Therefore, the Charpy impact energy can be presented as follows [22]:

$$CV = E_{plastic} + E_{fracture}, \tag{25}$$

where $E_{plastic}$ is the dissipated energy due to the plastic deformation, and $E_{fracture}$ is the absorbed energy from the crack initiation in the notch tip until the fracture.

2.1. ***Determining the Crack Initiation Energy***. Different criteria have been presented to predict the critical load for the notched specimens. Most of these criteria are usefull for brittle and quasi-brittle materials to predict the critical fracture load. These criteria can be used to determine the critical load (i.e., the load related to the crack initiation) for ductile materials. In the present work, the point stress (PS) criterion is used to determine the crack initiation point.

The PS criterion implies that fracture takes place when the circumferential stress $\sigma_{\theta\theta}$ at a specific critical distance $r_c$ from the notch tip reaches to its critical value $(\sigma_{\theta\theta})_c$. The critical value $(\sigma_{\theta\theta})_c$ can be taken to be equal to the ultimate tensile strength of the materilas, and the critical distance is calculated as follows [23]:

$$r_c = \frac{1}{2\pi}\left(\frac{K_{\mathrm{Ic}}}{\sigma_{UTS}}\right)^2, \tag{26}$$

where the fracture toughness $K_{\mathrm{Ic}}$ and the ultimate strength $\sigma_{UTS}$ are the material properties. Therefore, the critical distance $r_c$ is independent of the notch geometry. Since the mechanical properties of the FGS vary in the width direction, the critical distance $r_c$ [Eq. (26)] is derived from the following expression:

$$r_c = x_0 - a = \frac{1}{2\pi}\left(\frac{K_{\mathrm{Ic}}(x_0)}{\sigma_{UTS}(x_0)}\right)^2, \tag{27}$$

in which $a = 2$ mm is notch depth and $x_0$ is a distance between the critical point and the specimen edge. Solving Eq. (27), the values of $x_0$ and thereby $r_c$ would be obtained. In the simulated model, the loading of the specimen was increased gradually until the circumferential stress (i.e., stress component in direction perpendicular to notch bisector) for an element at distance $r_c$ from the notch tip equals to the critical stress related to the material including notch tip in the FG specimen.

2.2. ***Determining the Crack Propagation Energy***. In order to obtain the necessary energy related to the fracture of the specimen under mode I loading, a crack must propagate to create a crack surface $A_f$ in Fig. 6. Mathematically, the area $A_f$ would be obtained from the integration of the element $dA = Bdx$ from $x = a$ to $x = w$, in which $dx$ is the thickness of the element $dA$, while $a$, $B$, and $w$ are the notch depth, specimen thickness and specimen width, respectively, as illustrated by Fig. 6.

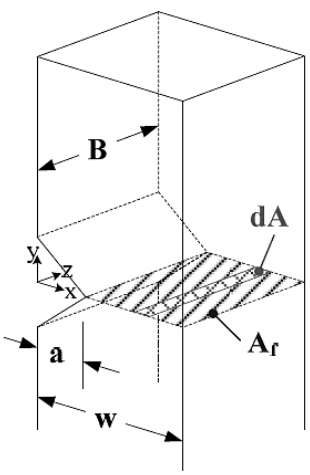


Fig. 6. The fracture area of the notched specimen.

With this assumption, the absorbed energy from the crack inititation time until the fracture time could be obtained utilizing the critical value of strain energy density as follows:

$$E_{fracture} = \int_{A_f} \left(\frac{dW}{dV}\right)_c (BdA), \tag{28}$$

where $(dW/dV)_c$ is the critical value of strain energy density to create the fracture area $dA$. The critical value of strain energy density depends on the materilas properties and can be expressed as follows [24]:

$$\left(\frac{dW}{dV}\right)_c = \frac{1}{2}\frac{\sigma_{UTS}^2}{E}. \tag{29}$$

Now, substituating Eq. (29) into Eq. (28) and considering the constant Young modulus in the composite, and exponential variation of the ultimate strength along the specimen width, Eq. (28) is transformed to the following equation:

$$E_{fracture} = \frac{B^2}{E}\frac{\sigma_{UTS}^2}{4}\frac{d+a}{\ln\left(\frac{\sigma_{UTS(2)}}{\sigma_{UTS(1)}}\right)}\left\{\left[\exp\left(\frac{2(w-a)}{d+a}\ln\left(\frac{\sigma_{UTS(2)}}{\sigma_{UTS(1)}}\right)\right)\right]-1\right\}. \tag{30}$$

3. **Results**.

3.1. ***The Comparision between the Charpy Impact Energy of FG and Homogeneous Steels***. In order to investigate the properties' gradient on the Charpy impact energy of composite, the variation of the Charpy impact energy for the FG steel $CV_{FG}$ versus the notch tip position obtained by Eq. (24) has been compared with those for the homogeneous steel with the same mechanical properties of the notch tip, $CV_H$. The mechanical properties of the boundary layers of the studied FGSs are shown in Table 1.

T a b l e 1

**The Mechanical Properties of the Single Phase Steels in the FGSs [6, 11, 25]**

| Mechanical property | Fracture toughness ($MPa \cdot m^{0.5}$) | Yield strength (MPa) | Ultimate tensile strength (MPa) | Charpy impact energy (J) |
|---|---|---|---|---|
| Original ferrite | 45.72 | 245 | 200 | 64 |
| Original austenite | 107.77 | 200 | 480 | 140 |
| Single-phase bainite | 82.08 | 1025 | 1125 | 108 |
| Single-phase martensite | 6.09 | 1440 | 1480 | 11 |

The variations of the Charpy impact energy vesus the notch tip position in different graded regions for both FG and homogeneous steels are given in Tables 2–4.

As Tables 2–4 show, in the austenitic region of both $\alpha\beta\gamma$ and $\gamma M\gamma$ composites, the impact energy of FG steel is less than that of a homogeneous steel with the same mechanical properties of the notch tip. This is due to the fact that the surrounding area for the notch tip plastic zone of the homogeneous steel is larger than that of the FG steel. Whereas, for ferritic region of $\alpha\beta\gamma$ composite, the impact energy of FG steel is larger than that of homogeneous steel because the surrounding area of the notch tip plastic zone of the FG steel is larger than the homogeneous steel. The maximum difference between the impact energy of the homogeneous and the FG steel was found about 26 J for the austenitic region of $\gamma M\gamma$ composite.

Table 2

**The Variation of the Impact Energy of the $\alpha\beta\gamma$ FG and Homogeneous Steels with the Same Mechanical Properties of the Notch Tip of FG Specimen Versus the Notch Tip Position when the Notch is in the Ferritic Region**

| The distance from notch tip to median layer of FG specimen (mm) | Charpy impact energy of FG steel $CV_{FG}$, J | Charpy impact energy of homogeneous steel $CV_H$, J | $\frac{CV_{FG}-CV_H}{CV_H}\cdot 100$, % |
|---|---|---|---|
| 1 | 2 | 3 | 4 |
| 0 | 110.7294 | 108.0000 | +2.52722 |
| 0.0001 | 110.0447 | 107.2787 | +2.57826 |
| 0.0002 | 109.3001 | 106.4935 | +2.63547 |
| 0.0003 | 108.4990 | 105.6476 | +2.69896 |
| 0.0004 | 107.6452 | 104.7448 | +2.76895 |
| 0.0005 | 106.7420 | 103.7885 | +2.84563 |
| 0.0006 | 105.7930 | 102.7823 | +2.92922 |
| 0.0007 | 104.8016 | 101.7295 | +3.01994 |
| 0.0008 | 103.7714 | 100.6336 | +3.11800 |
| 0.0009 | 102.7060 | 99.4985 | +3.22362 |
| 0.0010 | 101.6087 | 88.3275 | +3.33699 |
| 0.0011 | 100.4832 | 97.1243 | +3.45833 |
| 0.0012 | 99.3329 | 95.8925 | +3.58783 |
| 0.0013 | 98.1615 | 94.6357 | +3.72569 |
| 0.0014 | 96.9724 | 93.3575 | +3.87208 |
| 0.0015 | 95.7692 | 92.0618 | +4.02716 |
| 0.0016 | 94.5555 | 90.7520 | +4.19105 |
| 0.0017 | 93.3347 | 89.4320 | +4.36385 |
| 0.0018 | 92.1104 | 88.1055 | +4.54565 |
| 0.0019 | 90.8863 | 86.7762 | +4.73645 |
| 0.0020 | 89.6658 | 85.4478 | +4.93624 |
| 0.0021 | 88.4525 | 84.1243 | +5.14496 |
| 0.0022 | 87.2499 | 82.8093 | +5.36238 |
| 0.0023 | 86.0616 | 81.5068 | +5.58834 |
| 0.0024 | 84.8913 | 80.2204 | +5.82252 |
| 0.0025 | 83.7424 | 78.9542 | +6.06449 |
| 0.0026 | 82.6185 | 77.7120 | +6.31372 |
| 0.0027 | 81.5233 | 76.4977 | +6.56958 |
| 0.0028 | 80.4601 | 75.3152 | +6.83119 |
| 0.0029 | 79.4327 | 74.1684 | +7.09769 |
| 0.0030 | 78.4445 | 73.0614 | +7.36795 |
| 0.0031 | 77.4992 | 71.9981 | +7.64069 |
| 0.0032 | 76.6003 | 70.9824 | +7.91446 |
| 0.0033 | 75.7514 | 70.0186 | +8.18760 |
| 0.0034 | 74.9560 | 69.1104 | +8.45828 |
| 0.0035 | 74.2176 | 68.2621 | +8.72449 |
| 0.0036 | 73.5399 | 67.4777 | +8.98402 |
| 0.0037 | 72.9264 | 66.7613 | +9.23451 |
| 0.0038 | 72.3806 | 66.1171 | +9.47343 |

*Continued Table 2*

| 1 | 2 | 3 | 4 |
|---|---|---|---|
| 0.0039 | 71.9062 | 65.5491 | +9.69815 |
| 0.0040 | 71.5065 | 65.0616 | +9.90593 |
| 0.0041 | 71.1853 | 64.6587 | +10.09400 |
| 0.0042 | 70.9461 | 64.3446 | +10.25960 |
| 0.0043 | 70.7923 | 64.1236 | +10.39991 |
| 0.0044 | 70.7279 | 64.0000 | +10.51241 |

T a b l e 3

**The Variation of the Impact Energy of the $\gamma M \gamma$ FG and Homogeneous Steels with the Same Mechanical Properties of the Notch tip of FG Specimen Versus the Notch Tip Position when the Notch is in the Austenitic Region**

| The distance from notch tip to median layer of FG specimen (mm) | Charpy impact energy of FG steel $CV_{FG}$, J | Charpy impact energy of homogeneous steel $CV_H$, J | $\frac{CV_{FG} - CV_H}{CV_H} \cdot 100$, % |
|---|---|---|---|
| 1 | 2 | 3 | 4 |
| 0 | 10.9266 | 11.0000 | –0.66768 |
| 0.0001 | 12.8112 | 13.0115 | –1.53913 |
| 0.0002 | 14.7872 | 15.1374 | –2.31323 |
| 0.0003 | 16.8498 | 17.3745 | –3.01396 |
| 0.0004 | 18.9944 | 19.7156 | –3.65788 |
| 0.0005 | 21.2161 | 22.1594 | –4.25685 |
| 0.0006 | 23.5102 | 24.7006 | –4.81956 |
| 0.0007 | 25.8717 | 27.3348 | –5.35254 |
| 0.0008 | 28.2958 | 30.0574 | –5.86076 |
| 0.0009 | 30.7776 | 32.8638 | –6.34811 |
| 0.0010 | 33.3122 | 35.7494 | –6.81764 |
| 0.0011 | 35.8946 | 38.7095 | –7.27181 |
| 0.0012 | 38.5200 | 41.7392 | –7.71261 |
| 0.0013 | 41.1835 | 44.8337 | –8.14166 |
| 0.0014 | 43.8799 | 47.9878 | –8.56030 |
| 0.0015 | 46.6046 | 51.1967 | –8.96964 |
| 0.0016 | 49.3524 | 54.4552 | –9.37064 |
| 0.0017 | 52.1184 | 57.7579 | –9.76405 |
| 0.0018 | 54.8977 | 61.0997 | –10.15060 |
| 0.0019 | 57.6853 | 64.4751 | –10.53100 |
| 0.0020 | 60.4762 | 67.8787 | –10.90550 |
| 0.0021 | 63.2657 | 71.3049 | –11.27440 |
| 0.0022 | 66.0484 | 74.7480 | –11.63860 |
| 0.0023 | 68.8196 | 78.2023 | –11.99800 |
| 0.0024 | 71.5743 | 81.6621 | –12.35310 |
| 0.0025 | 74.3075 | 85.1212 | –12.70400 |
| 0.0026 | 77.0141 | 88.5739 | –13.05110 |
| 0.0027 | 79.6893 | 92.0139 | –13.39430 |
| 0.0028 | 82.3280 | 95.4351 | –13.73410 |

*Continued Table 3*

| 1 | 2 | 3 | 4 |
|---|---|---|---|
| 0.0029 | 84.9253 | 98.8313 | –14.0704 |
| 0.0030 | 87.4761 | 102.1960 | –14.4036 |
| 0.0031 | 89.9755 | 105.5227 | –14.7335 |
| 0.0032 | 92.4184 | 108.8049 | –15.0605 |
| 0.0033 | 94.7999 | 112.0360 | –15.3844 |
| 0.0034 | 97.1149 | 115.2092 | –15.7056 |
| 0.0035 | 99.3586 | 118.3177 | –16.0239 |
| 0.0036 | 101.5257 | 121.3544 | –16.3395 |
| 0.0037 | 103.6113 | 124.3124 | –16.6525 |
| 0.0038 | 105.6104 | 127.1845 | –16.9628 |
| 0.0039 | 107.5182 | 129.9634 | –17.2704 |
| 0.0040 | 109.3293 | 132.6418 | –17.5755 |
| 0.0041 | 111.0388 | 135.2121 | –17.8781 |
| 0.0042 | 112.6419 | 137.6671 | –18.1781 |
| 0.0043 | 114.1342 | 140.0000 | –18.4756 |

Table 4

**The Variation of the Impact Energy of the $\alpha\beta\gamma$ FG and Homogeneous Steels with the Same Mechanical Properties of the Notch Tip of FG Specimen Versus the Notch Tip Position when the Notch is in the Austenitic Region**

| The distance from notch tip to median layer of FG specimen (mm) | Charpy impact energy of FG steel $CV_{FG}$, J | Charpy impact energy of homogeneous steel $CV_H$, J | $\frac{CV_{FG}-CV_H}{CV_H}\cdot 100$, % |
|---|---|---|---|
| 1 | 2 | 3 | 4 |
| 0 | 105.9612 | 108.0000 | –1.88775 |
| 0.0001 | 106.3290 | 108.3908 | –1.90219 |
| 0.0002 | 106.7901 | 108.8828 | –1.92195 |
| 0.0003 | 107.3330 | 109.4640 | –1.94679 |
| 0.0004 | 107.9467 | 110.1232 | –1.97641 |
| 0.0005 | 108.6208 | 110.8495 | –2.01051 |
| 0.0006 | 109.3457 | 11.6327 | –2.04872 |
| 0.0007 | 110.1121 | 112.4633 | –2.09066 |
| 0.0008 | 110.9115 | 113.3322 | –2.13594 |
| 0.0009 | 111.7358 | 114.2308 | –2.18419 |
| 0.0010 | 112.5777 | 115.1513 | –2.23501 |
| 0.0011 | 113.4305 | 116.0866 | –2.28805 |
| 0.0012 | 114.2878 | 117.0298 | –2.34294 |
| 0.0013 | 115.1443 | 117.9750 | –2.39936 |
| 0.0014 | 115.9948 | 118.9166 | –2.45698 |
| 0.0015 | 116.8350 | 119.8499 | –2.51555 |
| 0.0016 | 117.6611 | 120.7707 | –2.57478 |
| 0.0017 | 118.4699 | 121.6754 | –2.63447 |
| 0.0018 | 119.2589 | 122.5612 | –2.69441 |
| 0.0019 | 120.0261 | 123.4258 | –2.75443 |

*Continued Table 4*

| 1 | 2 | 3 | 4 |
|---|---|---|---|
| 0.0020 | 120.7702 | 124.2676 | –2.81441 |
| 0.0021 | 121.4903 | 125.0856 | –2.87426 |
| 0.0022 | 122.1864 | 125.8796 | –2.93389 |
| 0.0023 | 122.8592 | 126.6502 | –2.99330 |
| 0.0024 | 123.5094 | 127.3982 | –3.05248 |
| 0.0025 | 124.1391 | 128.1257 | –3.11150 |
| 0.0026 | 124.7504 | 128.8351 | –3.17044 |
| 0.0027 | 125.3465 | 129.5296 | –3.22944 |
| 0.0028 | 125.9308 | 130.2131 | –3.28867 |
| 0.0029 | 126.5075 | 130.8902 | –3.34836 |
| 0.0030 | 127.0817 | 131.5665 | –3.40877 |
| 0.0031 | 127.6587 | 132.2480 | –3.47021 |
| 0.0032 | 128.2446 | 132.9415 | –3.53305 |
| 0.0033 | 128.8463 | 133.6548 | –3.59770 |
| 0.0034 | 129.4709 | 134.3960 | –3.66462 |
| 0.0035 | 130.1267 | 135.1745 | –3.73432 |
| 0.0036 | 130.8222 | 136.0002 | –3.80733 |
| 0.0037 | 131.5667 | 136.8836 | –3.88425 |
| 0.0038 | 132.3702 | 137.8364 | –3.96570 |
| 0.0039 | 133.2432 | 138.8707 | –4.05234 |
| 0.0040 | 134.1972 | 140.0000 | –4.14483 |

3.2. ***Validation of the Analytical Model for FG Composite***. In this paper, the FE analysis has been carried out to evaluate the accuracy of the analytical model. For example, when the notch tip is located in ferritic region of $\alpha\beta\gamma$ composite with 2 mm distance from the bainitic layer, the circumferential stress (i.e., $S_{11}$ in simulated model) in the deformed specimen is shown in Fig. 7. Due to symmetry, only a half of the model is shown.

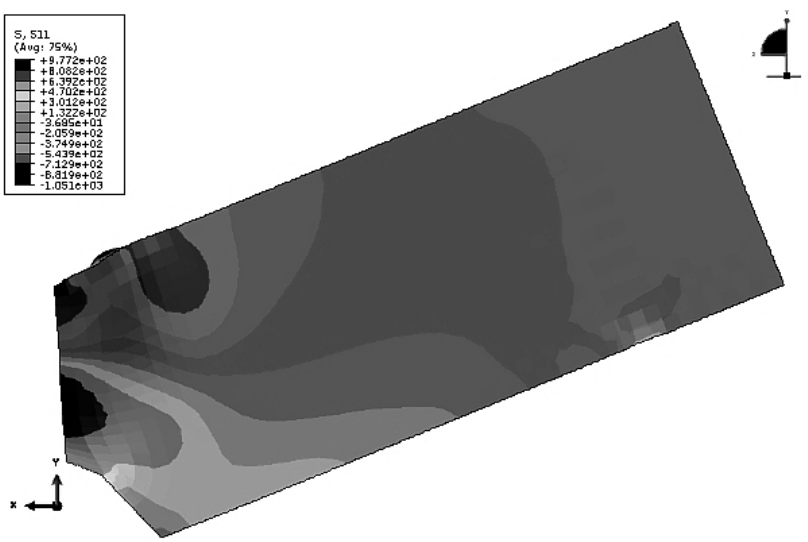


Fig. 7. The FE model after loading.

Notice that for this case, by solving Eq. (27), $x_0$ is obtained 0.003052 mm and then the crtical distance would be $r_c$ = 1.051805 mm. This means that the specimen deformation continues till the $\sigma_{\theta\theta}$ at the distance of 1.051805 mm from the notch tip reaches to the ultimate strength of the notch tip in the FG specimen. If this time is considered as the crack initiation point, the total energy of the specimen up to this time may be considred as the plastic dissipated energy $E_{plastic}$. Moreover, the fracture energy $E_{fracture}$ would be 4.46223 J by solving the Eq. (30). Therefore, the Charpy impact energy $CV_{FG}$ would be 89.6675 J according to the Eq. (25).

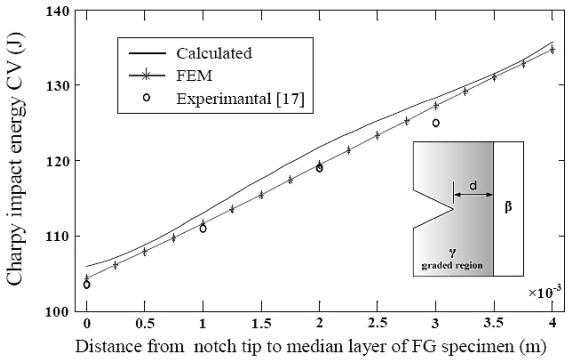


a

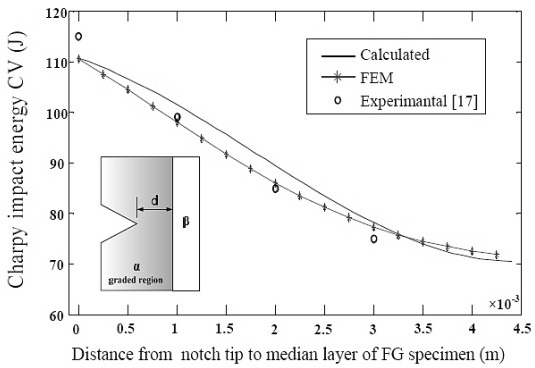


b

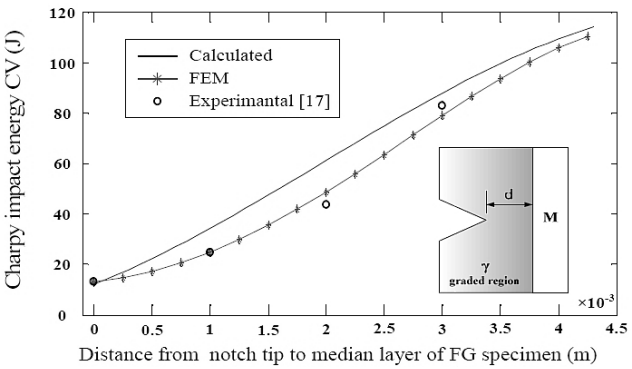


c

Fig. 8. The comparison between the Charpy impact energy obtained by the analytical model with FEM outputs and experimental ones when the notch tip is located at: (a) the ferritic region of the $\alpha\beta\gamma$; (b) the austenitic region of the $\alpha\beta\gamma$; (c) the austnitic region of the $\gamma M\gamma$.

The results of the analytical model for $\alpha\beta\gamma$ and $\gamma M\gamma$ FGSs versus the different position of the notch tip, as well as the finite element method (FEM) outputs, have been compared in Fig. 8. Moreover, the experimental values of the impact energy for four different notch tip positions have been cited from [17] and depicted by circular symbols in Fig. 8.

As this figure shows, there is a good agreement between the analytical model results with FEM outputs and experimental ones.

**Conclusions**. In this research, the Charpy impact energy of bainitic and martensitic FGSs produced via ESR process has been investigated both analyticaly, and by three-dimentional FEM simulation. The main findings of the paper are listed below:

1. An analytical model has been obtained to predict the Charpy impact energy of the FGS versus the notch tip position by correlating the Charpy impact energy of composite to the size of the notch tip plastic region.

2. The results show that in the transition region from original ferrite to median bainite layer of the $\alpha\beta\gamma$ FGS, the impact energy of the FG steel is higher than that of homogeneous steel with the same mechanical properties of the notch tip and for other regions the opposite situation is observed.

3. The results of the model were compared with the FEM results and the experimental ones taken from the literature. The sound agreement was found that demonstrated the proposed model potentials as a powerfull tool to predict impact behavior of FG steels.

**Р е з ю м е**

Функціонально-градієнтні сталі, що відносяться до групи функціонально-градієнтних матеріалів із пружно-пластичними властивостями, отримують із нержавіючої сталі шляхом електрошлакової переплавки. При використанні функціонально-градієнтних сталей можно поліпшити механічні властивості композитів із мартенситними і бейнітними крихкими фазами. Запропонована аналітична модель дозволяє оцінити ударну енергію руйнування зразків Шарпі з бейнітно-мартенситних сталей з урахуванням залежності між ударною енергією і розміром пластичної зони у вершині надрізу. Порівнюються величини ударної енергії для зразків Шарпі з функціонально-градієнтних сплавів та з однорідного матеріалу, що відповідає шару матеріалу біля вершини надрізу. Із використанням програмного комплексу ABAQUS виконано тривимірне скінченноелементне моделювання даного процесу. Згідно із законом Холломана, для пластичної зони отримано характеристики матеріалу в різних його шарах. Розглядалась експоненціальна зміна характеристик матеріалу по ширині зразка. Запропонована модель дозволяє отримати результати, які добре узгоджуються з відомими експериментальними даними і результатами скінченноелементних розрахунків.

1. R. Brighenti and A. Carpinteri, “Some considerations on failure of solids and liquids,” *Strength Mater*., **42**, No. 2, 154–166 (2010).
2. D. K. Jha, T. Kant, and R. K. Singh, “A critical review of recent research on functionally graded plates,” *Comp. Struct.*, **96**, 833–849 (2013).
3. B. Chehab, H. Zurob, D. Embury, et al., “Compositionally graded steels: A strategy for materials development,” *Adv. Eng. Mater*., **11**, No. 12, 992–999 (2009).
4. B. Skoczen, “Functionally graded structural members obtained via the low temperature strain induced phase transformation,” *Int. J. Solids Struct.*, **44**, 5182–5207 (2007).
5. J. Aghazadeh Mohandesi and M. H. Shahosseini, “Transformation characteristics of functionally graded steels produced by electroslag remelting,” *Met. Mater. Trans. A*, **36**, 3471–3476 (2005).

6. J. Aghazadeh Mohandesi, M. H. Shahosseinie, and R. Parastar Namin, "Tensile behavior of functionally graded steels produced by electroslag remelting," *Met. Mater. Trans. A*, **37**, 2125–2132 (2006).
7. A. Nazari, J. Aghazadeh Mohandesi, and S. Tavareh, "Microhardness profile prediction of a graded steel by strain gradient plasticity theory," *Comput. Mater. Sci.*, **50**, 1781–1784 (2011).
8. A. Nazari, J. Aghazadeh Mohandesi and S. Tavareh, "Modeling tensile strength of austenitic graded steel based on the strain gradient plasticity theory," *Comput. Mater. Sci.*, **50**, 1791–1794 (2011).
9. M. Abolghasemzadeh, H. Samareh Salavati Pour, F. Berto, and Y. Alizadeh, "Modeling of flow stress of bainitic and martensitic functionally graded steels under hot compression," *Mater. Sci. Eng. A*, **534**, 329–338 (2012).
10. E. Barati, Y. Alizadeh, and J. Aghazadeh Mohandesi, "J-integral evaluation of austenitic–martensitic functionally graded steel in plates weakened by U-notches," *Eng. Fract. Mech*., **77**, 3341–3358 (2010).
11. A. Nazari and J. Aghazadeh Mohandesi, "Impact energy of functionally graded steels with crack divider configuration," *J. Mater. Sci. Technol.*, **25**, 847–852 (2009).
12. A. Nazari and J. Aghazadeh Mohandesi, "Modeling impact energy of functionally graded steels in crack divider configuration," *Mater. Sci. Technol.*, **26**, 1377–1383 (2010).
13. A. Nazari, J. Aghazadeh Mohandesi, and S. Riahi, "Modeling impact energy of functionally graded steels in crack divider configuration using modified stress–strain curve data," *Int. J. Damage Mech.*, **21**, 27–50 (2012).
14. A. Nazari and S. M. M. Najafi, "Prediction Charpy impact energy of bcc and fcc functionally graded steels in crack divider configuration by strain gradient plasticity theory," *Comput. Mater. Sci.*, **50**, 3178–3183 (2011).
15. A. Nazari, "Application of strain gradient plasticity theory to model Charpy impact energy of functionally graded steels," *Comput. Mater. Sci.*, **50**, 3410–3416 (2011).
16. A. Nazari, "Application of strain gradient plasticity theory to model Charpy impact energy of functionally graded steels using modified stress–strain curve data," *Comput. Mater. Sci.*, **51**, 281–289 (2012).
17. A. Nazari and J. Aghazadeh Mohandesi, "Impact energy of functionally graded steels in crack arrester configuration," *J. Mater. Eng. Perform*., **19**, 1058–1064 (2010).
18. A. A. Baron, "A thermodynamic model for fracture toughness prediction," *Eng. Fract. Mech.*, **46**, 245–251 (1993).
19. C. H. Gür and I. Yildiz, "Non-destructive investigation on the effect of precipitation hardening on impact toughness of 7020 Al-Zn-Mg alloy," *Mater. Sci. Eng. A*, **382**, 395–400 (2004).
20. R. W. Hertzberg, *Deformation and Fracture Mechanics of Engineering Materials*, 4th edition, John Wiley, New York (1996).
21. V. Leskovšek, B. Ule, and B. Liščić, "Relations between fracture toughness, hardness and microstructure of vacuum heat-treated high-speed steel," *J. Mater. Process. Technol.*, **127**, 298–308 (2002).
22. G. C. Sih and D. Y. Tzou, "Dynamic fracture of Charpy V-notch specimen," *Theor. Appl. Fract. Mech.*, **5**, 189–203 (1986).
23. M. R. Ayatollahi and A. R. Torabi, "Brittle fracture in rounded-tip V-shaped notches," *Mater. Des*., **31**, 60–67 (2010).

24. P. Lazzarin and R. Zambardi, "A finite-volume-energy based approach to predict the static and fatigue behavior of components with sharp V-shaped notches," *Int. J. Fract.*, 112, 275–298 (2001).

25. J. Aghazadeh Mohandesi, A. Nazari, M. H. Vishkasogheh, and M. Abedi, "Modeling fracture toughness of functionally graded steels in crack divider configuration," *Modell. Simul. Mater. Sci. Eng.*, **18**, 1–13 (2010).

Received 15. 01. 2014